Zitierweise: *Angew. Chem. Int. Ed.* **2024**, *63*, e202409503
doi.org/10.1002/anie.202409503

Raman Spectroscopy

The Coking of a Solid Catalyst Rationalized with Combined Raman and Fluorescence Lifetime Microscopy

*Robin Vogel, Caroline Versluis, Rowie Frijsen, P. Tim Prins, Eelco T. C. Vogt, Freddy T. Rabouw, and Bert M. Weckhuysen**

Abstract: The formation of carbon deposits is a major deactivation pathway for solid catalysts. Studying coking on industrially relevant catalysts is, however, often challenging due to the sample heterogeneity. That is especially true for zeolite-containing catalysts where fluorescence often hampers their characterization with Raman spectroscopy. We turned this disadvantage into an advantage and combined Raman and fluorescence (lifetime) microscopy to study the coking behavior of an equilibrium catalyst material used for fluid catalytic cracking of hydrocarbons. The results presented illustrate that this approach can yield new insights in the physicochemical processes occurring within zeolite-containing catalyst particles during their coking process. Ex situ analyses of single catalyst particles revealed considerable intra-sample heterogeneities. The sample-averaged Raman spectra showed a higher degree of graphitization when the sample was exposed to more hexane, while the sample-averaged fluorescence lifetime showed no significant trend. Simultaneous in situ Raman and fluorescence (lifetime) microscopy, used to follow the coking and the regeneration of single particles, gave more insights in the changing fluorescence dynamics. During the coking, the rise and decline of the average fluorescence lifetime suggested the prolonged presence of smaller coke species that are quenched more and more by adjacent larger polyaromatics acting as Förster-resonance-energy-transfer acceptors.

[*] R. Vogel, C. Versluis, R. Frijsen, Dr. P. T. Prins, Dr. E. T. C. Vogt, Dr. F. T. Rabouw, Prof. Dr. B. M. Weckhuysen
Inorganic Chemistry and Catalysis Group, Institute for Sustainable and Circular Chemistry and Debye Institute for Nanomaterials Science, Utrecht University, Universiteitsweg 99, 3584 CG Utrecht, The Netherlands
E-mail: b.m.weckhuysen@uu.nl

Dr. F. T. Rabouw
Soft Condensed Matter Group, Debye Institute for Nanomaterials Science, Utrecht university, Princetonplein 1, 3584 CC Utrecht, The Netherlands

Introduction

The formation of carbon deposits (further denoted as coke) is a major deactivation pathway for solid hydrocarbon-conversion catalyst materials. It is known that coke blocks the catalyst active sites and clogs the catalyst pores hampering the continuous conversion of hydrocarbon feedstock, such as crude oil and pyrolysis oil fractions, into valuable chemicals. Regeneration of the deactivated catalyst material partially restores its catalytic activity, although this process leads to irreversible changes to the solid catalyst.[1] Coking can be investigated with a wide variety of bulk analytical techniques, including spectroscopy and microscopy techniques. An in-depth understanding of the underlying mechanisms of coke formation during catalysis can mitigate reversible and irreversible catalyst deactivation phenomena, especially when the coking process is studied in situ or operando under realistic working conditions.[2]

Catalyst coking studies for the industrially important process of fluid catalytic cracking (FCC) are challenging because of the complexity and heterogeneity of the catalyst. FCC is a key refinery process where vacuum gas oil (VGO) is converted into lower olefins and gasoline-range hydrocarbons.[3] More recently, FCC catalyst materials are also explored for the cracking of plastic waste, such as polypropylene.[4–6] The cracking of carbon–carbon bonds is facilitated by FCC catalyst particles composed of multiple components, including zeolites, clay, silica, and alumina. The zeolite material, most often ultra stable zeolite Y (USY), provides the active acid sites, while clay acts as a heat sink, and silica and alumina binder materials provide meso- and microporosity, making the catalyst particle accessible for larger molecules. The components are mixed in a slurry and subsequently spray-dried to form the spherical particles with a 50–75 μm diameter that are used in petrochemical industry. The harsh conditions in a cracking reactor, during thousands of consecutive cracking and regeneration cycles, cause long-term, irreversible catalyst deactivation. In practice, the lifetime of an FCC catalyst particle is about one month and a fraction of the catalyst is replaced with fresh catalyst at regular intervals. This results in a broad steady-state lifetime distribution of the catalyst particles, also termed equilibrium catalyst (further denoted as E-cat).[1,3]

The buildup of carbon deposits within and on the outer surface of FCC catalysts is due to the formation of carbon-rich byproducts during cracking, hydrogenation–dehydrogenation on poisoning metals, incomplete regeneration, and the deposition of large aromatic hydrocarbons from the

feed.[7] The fast catalytic formation of coke starts when small molecules undergo alkylation, isomerization, and dehydrogenation to form toluene, which can grow further into polyaromatic species.[2,8] Analyses of the 3D distribution and the nature of coke on the surface and in the pore space of a FCC catalyst particle with X-ray nanotomography and nuclear magnetic resonance (NMR) revealed that outer surface coke is relatively aromatic, while coke within the catalyst particle pore space is more aliphatic in nature.[7,9]

Raman spectroscopy has been used to probe the nature of the carbonaceous species that accumulate on the surface of the catalyst. Typical Raman spectra of coked samples show G- and D-bands due to graphitic carbon and the defects in graphitic carbon, respectively. The relative intensities of these bands reveal the degree of graphitization. In practice, Raman spectroscopy has been used for the analysis of FCC catalyst material[10] to follow the degree of graphitization within series of catalysts with increasing amounts of coke[11,12] or increasing age.[13] However, it is challenging to establish significant trends within a series due to the heterogeneous nature of the samples.[14]

Confocal fluorescence microscopy (CFM), another technique based on laser excitation, has been used to reveal the distribution and the nature of aromatic species on a single-particle level. For example, the brightness of fluorescence emitted by deactivating species was found to correlate with the location of the active zeolitic material in single FCC particles.[15] The redshift of the fluorescence, recorded in situ during the alcohol-to-olefins reaction, was attributed to the formation of more extended coke.[16] Indeed, fluorescence redshifts with extended conjugation, although the precise molecular structure of the polyaromatic molecule also influences the fluorescence.[17] Another characteristic metric of fluorescence is its lifetime, but this feature has not been explored in-depth for the study of catalyst coking.[18–22] It is difficult to relate the fluorescence lifetime of polyaromatic hydrocarbons directly to their molecular structure, because it is also strongly affected by the interplay between the excited fluorophore and its environment.[23–27] Coked catalysts are solids covered with a highly complex mixture of carbonaceous species. This makes the chemical interpretation of fluorescence lifetime measurements on coked catalysts challenging.[28]

In this work, we combine Raman and fluorescence (lifetime) microscopy to study the coking behavior of an E-cat material. Combining these three microscopy techniques provides a detailed picture of the coking of this showcase material, which exhibits a compositional complexity often encountered in industrial hydrocarbon-conversion catalysts. Therefore, this study provides a new approach to assess the coke formation processes for a wide variety of industrial catalysts. We first analyze a large set of single E-cat particles ex situ in a series of samples coked with an increasing number of hexane pulses. Excitation with a pulsed laser induces both Raman scattering and fluorescence. The collected signal is split over two detectors,[29–33] which allows to record spectra and fluorescence lifetimes simultaneously. This ex situ analysis shows considerable intra-sample heterogeneities. Both the degree of graphitization and the fluorescence lifetime vary greatly from catalyst-particle to catalyst-particle within a sample. Averaging 75 measurements per sample clearly reveals a higher degree of graphitization for samples more exposed to hexane and hints on an interesting evolution of the fluorescent lifetime. The trends are confirmed with in situ measurements, thereby offering new insights in the relationship between the type of coke molecules and their fluorescence lifetimes.

Results and Discussion

Raman and Fluorescence Lifetime Microscopy for Single Catalyst Particle Analysis

We prepared a series of coked samples from E-cat material and analyzed them with combined Raman and fluorescence lifetime microscopy. The catalyst material was heated up to 600 °C and dosed with 10, 24, 50, and 100 pulses of 0.1 μL hexane. Figure 1 illustrates how single particles of the E-cat sample coked with 5.0 μL hexane were analyzed with Raman and fluorescence lifetime microscopy. Figure 1a provides a schematic overview of the combined method. Pulsed laser excitation is used to probe individual coked E-cat particles. The induced Raman scattering and fluorescence signals emanating from these individual catalyst particles are split and sent to a charge-coupled device (CCD) detector for a spectral measurement, while the fluorescence decay dynamics is analyzed with single-photon avalanche diode (SPAD)-based time gating.

The initial visual inspection with the optical microscope, shown in Figure 1b, revealed large variations in catalyst particle sizes and shapes, ranging from spherical to more anisotropic. In addition, the colors of the catalyst particles ranged from light grey to black. These catalyst-particle-to-catalyst-particle variations can be attributed to the broad age distribution of the particles within the E-cat sample and compositional inhomogeneity due to a non-uniform distribution of catalyst components. Some catalyst particles are relatively fresh and active, having spherical shapes and showing high coking activity yielding graphitic black carbon on the surface (Figure 1c). On the other hand, some catalyst particles might be relatively old, damaged and deactivated, resulting in anisotropic particles showing little coking activity keeping the particles relatively light gray (Figure 1d–e).[34,35] The comparison of the reflection images shows that it is imperative to assess sample heterogeneity before drawing conclusions about data originating from only a few E-cat particles within a sample.

Figure 1f compares three normalized Raman spectra recorded on the E-cat sample coked with 5.0 μL hexane. The presented spectra show G- and D-bands due to ring breathing modes of graphitic sheets and their edges and defects, respectively. In addition, broad background fluorescence due to laser-induced electronic transitions in aromatic coke species is observed. Typically, the degree of graphitization of the carbon deposits is interpreted from the D-to-G-band intensity ratio.[10–14] A higher ratio implies a large number of graphitic edges and defects, suggesting that

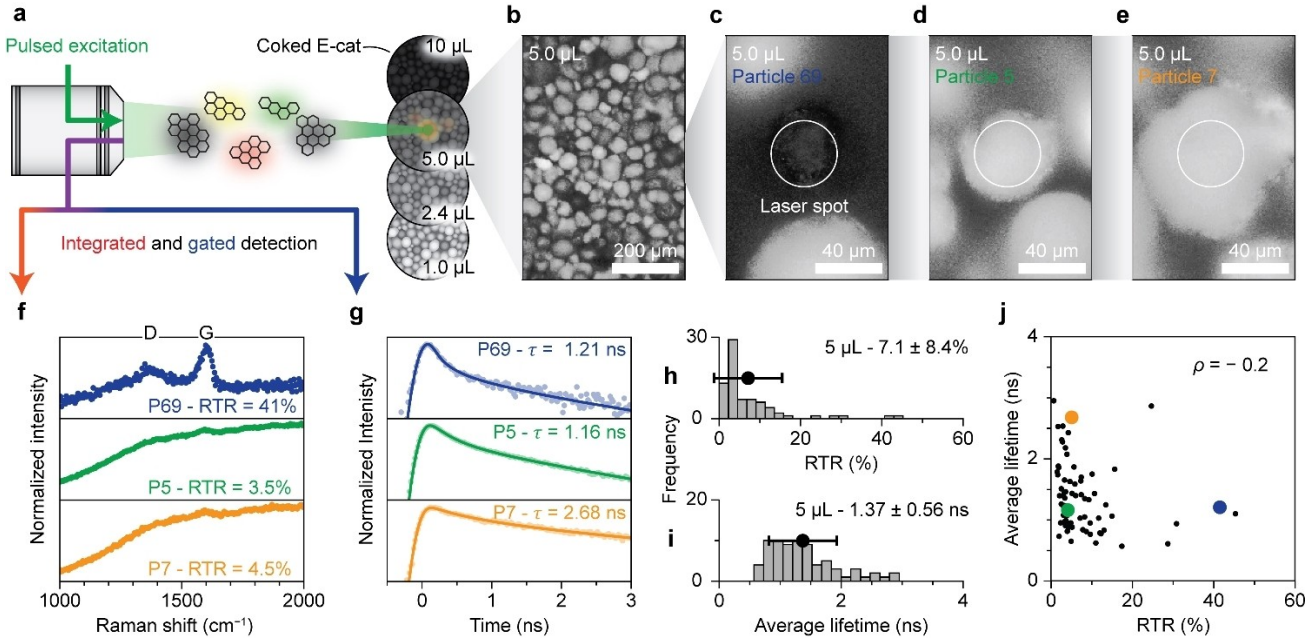

Figure 1. Ex situ Raman and fluorescence lifetime microscopy for single-particle analysis of E-cat material coked with 5 µL hexane. (a) Schematic overview of the combined Raman and fluorescence lifetime microscopy method. (b) Overview reflection image of the E-cat sample coked with 5 µL hexane. (c–e) Reflection images of particles 69, 5, and 7, respectively. The white circles represent the laser spot with a 41 µm diameter. (f) Comparison of the normalized Raman spectra of particles 5, 7, and 69. The spectra are normalized on the maximum of the G-band, centered around 1600 cm^{-1} and shown between 0.2 and 1.1. (g) Comparison of the normalized fluorescence decay traces of particle 5, 7, and 69. The traces are normalized on the maximum and shown between 0.015 and 1.5 on a logarithmic *y*-scale. The experimental datapoints are shown together with the results of the fitting procedure and the obtained weighted average fluorescence lifetime ($\bar{\tau}$) (Figure S3). (h) Histogram with the distribution of the Raman-to-total ratio (RTR) of the 75 particles of the sample. (i) Histogram with the distribution of $\bar{\tau}$ of the 75 particles of the sample. (j) Comparison of RTR and $\bar{\tau}$ of the 75 particles recorded on the sample. Particles 5, 7, and 69 are highlighted in green, yellow, and blue, respectively.

graphitic patches are relatively small compared to samples with a lower D-to-G ratio. Quantifying the areas of the bands of interest is complicated because of the broad background fluorescence, especially the broad D-band is indistinguishable from the background in spectra with relative weak Raman contribution with respect to fluorescence. Therefore, we use the Raman-to-total ratio (RTR) as a metric for the degree of graphitization of the coke instead of the D-to-G ratio. The RTR is defined as the ratio of the amplitude of the G-band above the background to the total signal at the wavelength of the G-band (Figure S2). A lower RTR can be due to a small amount of Raman scattering graphitic carbon deposits or intense background fluorescence or both, whereas a higher RTR can be due to a large amount of Raman scattering species or weak background fluorescence or both. Catalyst particle 69 has a RTR of 41 %, whereas the other catalyst particles show much weaker Raman signal (RTR = 3.5 % for particle 5 and 4.5 % for particle 7). Overall, the particles coked with 5.0 µL of hexane have a RTR of 7.1 ± 8.4 % (mean ± standard deviation over 75 particles). The histogram of the RTR distribution, presented in Figure 1h, further underlines the heterogeneity of the sample.

The fluorescence decay dynamics of the signal recorded between 538 and 596 nm is illustrated with time traces in Figure 1g. The pulsed laser induces fast processes–instantaneous Raman scattering and sub-ns fluorescence indistinguishable from each other–and slower fluorescence characterized by exponential decay. Therefore, the time traces were fit to the sum of the instrument response function (IRF) describing the fast processes and two components describing fluorescence. The fluorescence components are described with the convolution of the IRF with exponential decay (Figure S3). A coked sample typically contains a wide variety of polyaromatic hydrocarbons that fluoresce with a broad range of different lifetimes.[8,23,24] Here, two exponential components were sufficient to match the data accurately, so we report the weighted average fluorescence lifetime ($\bar{\tau}$) of the two components. Comparing $\bar{\tau}$ from catalyst-particle to catalyst-particle reveals large variations. Catalyst particle 5 exhibits a $\bar{\tau}$ of 1.16 ns, whereas catalyst particle 7 has a $\bar{\tau}$ of 2.68 ns. The fluorescence decay traces of catalyst particles 7 and 69 appear different due to the relatively large contribution of the IRF for catalyst particle 69. The average lifetime values observed for the 5.0 µL sample are distributed over 1.37 ± 0.56 ns, as shown by the histogram in Figure 1i.

Figure 1j reveals that the RTR and the $\bar{\tau}$ are not correlated. Indeed, catalyst particles 5 and 7 exhibit a different $\bar{\tau}$ value, but a similar RTR value. Furthermore, catalyst particles 5 and 69 have a similar $\bar{\tau}$ value, but a different RTR value. This indicates that Raman and fluorescence lifetime microscopy are complimentary analytical techniques to assess the properties of coke deposits. The considerable intra-sample variations are probably due to the

broad age distribution or compositional inhomogeneity of the E-cat material used for the coking experiments.

Sample-averaged Raman and Fluorescence Lifetime Microscopy

Figure 2 shows that trends in the Raman and fluorescence lifetime microscopy data for the series of E-cat materials pulse-coked with 1.0, 2.4, 5.0, and 10 µL hexane can be established when averaging over a large number of catalyst particles. The overview reflection images presented in Figure S4 show heterogeneous samples that darken with increased hexane exposure, indicating the increased coke deposition. In addition, the thermogravimetric analysis (TGA), as presented in Figure S5, showed the buildup of carbon deposits with increased hexane doses. The extended and heterogeneous coke formation was further studied with Raman and fluorescence lifetime microscopy.

The RTR histograms, presented in Figure 2a, illustrate the broad distribution of graphitization within each sample. Nevertheless, the distributions clearly shift to higher RTR with increasing hexane exposure. The average normalized Raman spectra in Figure 2b provide an alternative visualization of this trend. The D- and G-bands become more pronounced with respect to background fluorescence upon increased hexane exposure, indicating that the Raman scattering of graphitic coke becomes more dominant over the background fluorescence due to the relative lower amount of smaller aromatic-type molecules.

The average lifetime histograms, shown in Figure 2c, also show broad distributions within each sample, but a trend is discernable. With increasing degree of coking, $\bar{\tau}$ tends to increase initially and then decrease. However, the large standard deviation on $\bar{\tau}$ makes it difficult to determine if the differences in the mean $\bar{\tau}$ between the 1.0, 2.4, and 5.0 µL samples are significant. For the 10 µL sample, $\bar{\tau}$ is however clearly shorter. The averaged normalized fluorescence time traces, as shown in Figure 2d, provide another visualization of the development of the average $\bar{\tau}$ from sample to sample. The slope of the fluorescence decay of the 1.0, 2.4, and 5.0 µL samples varies slightly while the 10 µL sample clearly shows fluorescence with a shorter $\bar{\tau}$.

The observed heterogeneity of the E-cat samples complicates the establishment of trends in the data that can facilitate the rationalization of the formation of coke. Comparing the RTR and $\bar{\tau}$ values of the coked E-cat samples in Figure S6 reveals that the two descriptors are not correlated. Averaging the Raman measurements over 75 catalyst particles brings out the increased graphitization of coke with more hexane exposure while clear developments in the fluorescence dynamics are difficult to prove. Interestingly, the TGA analysis showed only a small difference in the amount of carbon deposits for the studied samples (Figure S5). The E-cat materials coked with 1.0, 2.4, 5.0, and 10 µL hexane were composed of 0.57, 0.67, 0.70, and 1.34 % carbon deposits respectively. On the other hand, the microscopy data clearly revealed differences in the degree of graphitization of carbon deposited on the E-cat particles.

In situ Raman and Fluorescence Lifetime Microscopy

In situ spectroscopy of individual E-cat particles provides insight on the different coking stages that is not obscured by catalyst-particle-to-catalyst-particle variations. Figure 3 illustrates the tracking of single E-cat particles during hexane cracking experiments using simultaneous in situ Raman and fluorescence (lifetime) microscopy.

The heatmap of the normalized Raman spectra recorded during the coking of catalyst particle 1, presented in Figure 3a, shows that the D- and G-bands become more prominent with respect to the fluorescence background over time. Indeed, the RTR increases to 17 % during the 35 min of hexane cracking. The carbon deposits formed within the E-cat particle grow from aromatic-type molecules into graphitic-type sheets, changing from (more dominantly) fluorescent species to (more dominantly) Raman scattering species to consequently increase the RTR values. Tracking

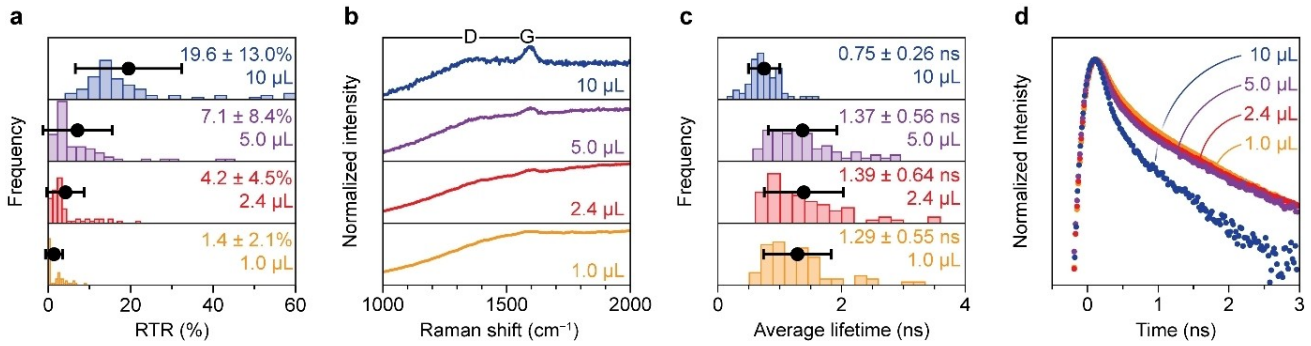

Figure 2. Ex situ sample-averaged Raman and fluorescence lifetime microscopy on E-cat materials pulse-coked with 1.0, 2.4, 5.0, and 10 µL hexane. (a) Histograms with the distributions of the RTR of the 75 particles measured per sample. (b) Averaged normalized Raman spectra of the samples under study. The spectra are normalized on the maximum of the G-band, centered around 1600 cm^{-1} and shown between 0.3 and 1.1. (c) Histograms with the $\bar{\tau}$ distribution of the 75 particles measured per sample. (d) Averaged normalized fluorescence time traces of the samples under study. The time traces are normalized on the maximum and shown on a logarithmic *y*-scale between 0.015 and 1.5. The black points and error bars in the histograms represent the average and the standard deviation.

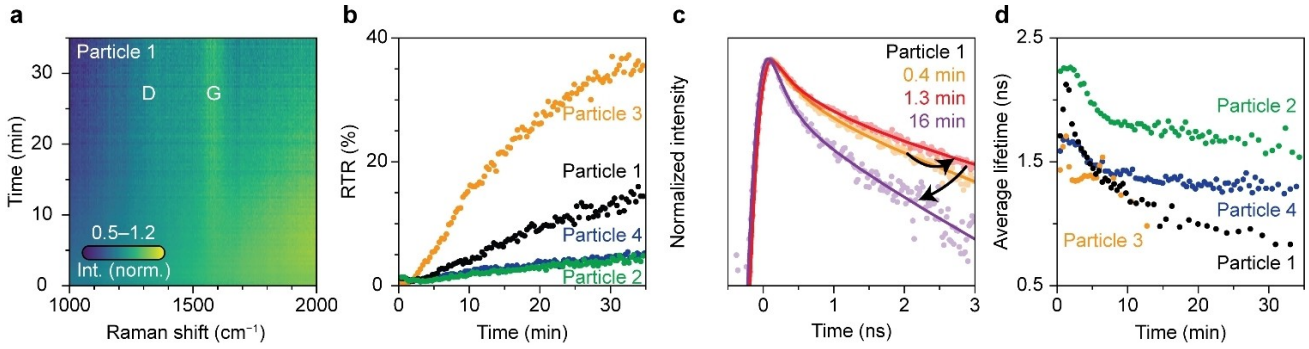

Figure 3. Simultaneous single-particle in situ Raman and lifetime microscopy during hexane cracking over calcined E-cat material. (a) Heatmap of the Raman spectra of E-cat particle 1 recorded with the Raman spectrometer over the course of 35 min of hexane cracking. At each time, the spectrum is normalized to the maximum of the G-band, centered around 1600 cm^{-1}. (b) RTR as a function of time for four catalytic runs. (c) Normalized fluorescence decay traces recorded after 0.4, 1.3, and 16 min of hexane cracking during run 1 recorded with the time-gated spectrometer. The decay traces are normalized on the maximum and shown on a logarithmic y-scale between 1.5 and 0.015. The experimental datapoints are shown together with the results of the fitting procedure. (d) $\overline{\tau}$ as a function of experimental time for the four catalytic runs. The low-intensity fluorescence time traces were summed consecutively to exceed a threshold intensity to fit the time-trace model accurately to the data. As a result, $\overline{\tau}$ of particle 3 is only reported over the course of 15 min.

the RTR of more E-cat particles over time, as shown in Figure 3b, clearly illustrates increasing graphitization of the coke deposits for all catalyst particles. In all four runs, the RTR increases, reaching 5 % in run 2 and 4, while the RTR reaches 35 % in run 3. The graphitization rates of run 2 and 3 differ by more than a factor 13 (determined from the slope of the RTR data between 5 and 10 min). The different rates can be attributed to the differences in catalytic activity from particle to particle in the E-cat mixture.

The change in fluorescence dynamics over time during the coking of an E-cat particle is shown in Figure 3c. The fluorescence decay initially slows down over the first 1.4 minutes before accelerating, indicating a lengthening followed by a shortening of the $\overline{\tau}$ value. This kinetic behavior is observed in all four catalyst particles investigated, as depicted in Figure 3d.

The rationalization of the fluorescence lifetime trend, as illustrated in Figure 4, can yield further insights in the physicochemical events occurring within the E-cat particles. Figure 4a reveals that the fluorescence emission redshifts over time, indicating the growth of polyaromatic species. Assigning features in the fluorescence spectrum of this extremely heterogeneous sample to specific polyaromatic hydrocarbons is difficult. Not only the size but also the particular molecular structure of a polyaromatic molecule influences its fluorescence (Figure S7).[17] In this work, $\overline{\tau}$ is recorded in a limited wavelength window, between 538 and 596 nm. Therefore, the $\overline{\tau}$ values represent those of polyaromatic hydrocarbons with a limited size range, most probably of 20 to 50 carbon atoms depending on the type and size of the hydrocarbon molecule. Plausible emitters are tetracene, terrylene, or a benzoid containing 10 electron sextets.[17] Such limited-size hydrocarbons emit green/yellow

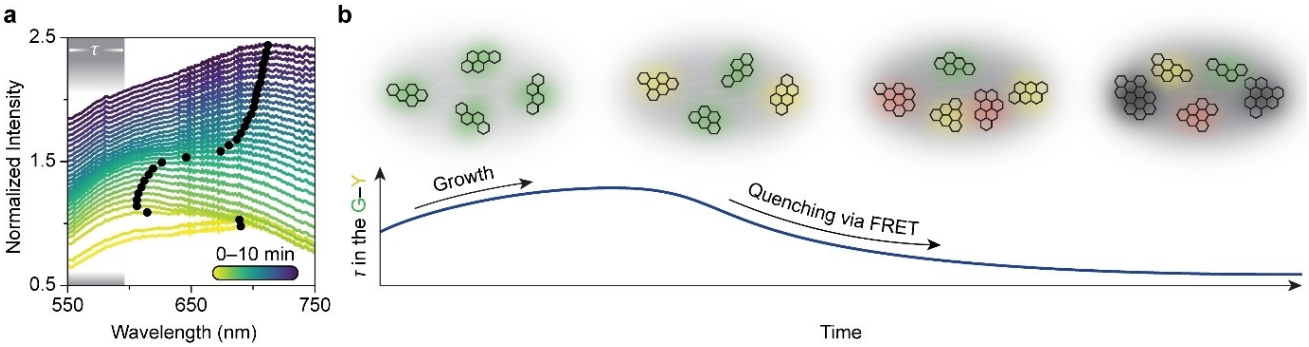

Figure 4. Rationalization of the changing fluorescence dynamics during the coking of E-cat. (a) Fluorescence emission spectra of particle 1 recorded with the Raman spectrometer during the hexane cracking experiment. The spectra are normalized on their maximum and plotted with a 0.05 offset. The black points indicate the maximum of the spectra. The grey area illustrates the wavelength range of the fluorescence lifetime measurement, corresponding to molecules emitting in the green and yellow spectral region. (b) Simplified representation of the formation and growth of polyaromatic molecules on the surface of an E-cat particle to explain the changing fluorescence dynamics. The initial growth of green emitters can increase the detected $\overline{\tau}$ in the green and yellow spectral region. Further growth of polyaromatic molecules near the green and yellow emitters can quench their luminescence via FRET to decrease the detected $\overline{\tau}$. The drawn molecular structures are not suggestions for the assignment of the data to specific molecules, but rather a suggestion for the trends in the growth of polyaromatic and graphitic structures.

fluorescence, while larger ones emit outside the detection window of our fluorescence lifetime setup. A simplified illustration of the formation and growth of green/yellow-emitting polyaromatic hydrocarbons in the proximity of other larger polyaromatic hydrocarbons is provided in Figure 4b. The initial limited growth from green to yellow emitters might correlate with the increased $\overline{\tau}$ value because radiative decay slows down as fluorescence redshifts.[18] Further growth of some polyaromatic hydrocarbons within the measured ensemble of species advances the fluorescence redshift. These red emitters are undetectable for the lifetime measurements. In the meantime, some green and yellow emitters might maintain their molecular sizes. In time, more and more graphitic-type structures form indicated by the rising RTR (Figure 3b). The red emitters and the graphitic-type structures influence the fluorescence lifetime of remaining green/yellow emitters by Förster resonance energy transfer (FRET). FRET from an excited green/yellow emitter to nearby larger and graphitic-type structures provides an additional decay pathway for the excited state, and thereby decreases the fluorescence lifetime.[18–21] The decreasing $\overline{\tau}$ after 2 min of coking (Figure 3d) thus evidences an increasing amount of larger and more graphitic-type structures.

Combined in situ Raman and fluorescence (lifetime) microscopy provides a more detailed picture of the coking behavior of an industrially relevant E-cat material. The growth of polyaromatic species into graphitic-type carbon is illustrated by the fluorescence redshift and the increasing RTR. The fluorescence lifetime measurements indicate the prolonged presence of smaller fluorescent hydrocarbons of which the emission is most probably quenched progressively by nearby larger polyaromatics that act as FRET acceptors. The technique developed here was also used to investigate the regeneration of coked E-cat particles to reveal the breaking of larger graphitic coke structures and the cleansing of the catalytic surface, as presented in Figure S8. During the regeneration, the D- and G-bands become less prominent with respect to the fluorescence background, indicating the breaking down of larger, graphitic structures into smaller polyaromatic hydrocarbons. These species shrink over time, indicated by a fluorescence blueshift. Furthermore, $\overline{\tau}$ lengthens during the regeneration. Here, the clearance of the catalyst surface, due to the combustion of coke molecules, might also influence the lifetime of green/yellow emitters due to FRET. Additional decay pathways for excited green/yellow emitters via FRET to nearby larger structures become less and less available, increasing $\overline{\tau}$.

Conclusion

The combination of Raman and fluorescence (lifetime) microscopy was used to study the coking and the regeneration of an industrially relevant refinery catalyst, more specifically an E-cat material. The ex situ post-mortem analyses of single catalyst particles from the E-cat sample coked with 5.0 μL of hexane illustrated considerable intra-sample heterogeneities in the type and amount of coke deposits. Both the degree of graphitization and the fluorescence dynamics vary substantially from catalyst particle-to-catalyst particle. Interestingly, the degree of graphitization of the coke deposits, as inferred from the Raman-to-total ratios (RTR) and the weighted average fluorescence lifetime ($\overline{\tau}$) of the E-cat particles within one sample are not correlated. The lack of correlation indicates that the two microscopy techniques yield complementary insights on the chemical nature of the carbon deposits formed within the catalyst material.

The ex situ sample-averaged analyses of the series of coked E-cat samples prepared with 1.0, 2.4, 5.0, and 10 μL hexane revealed interesting trends. Averaging the Raman spectra and fluorescence time traces of the 75 measured catalyst particles per sample showed a higher degree of graphitization when the sample was exposed to more hexane. The sample-averaged $\overline{\tau}$ suggested the tendency of $\overline{\tau}$ to increase initially, followed by a decrease, but the differences between samples were small compared to the observed intra-sample heterogeneities. These results show that the microscopy techniques are only useful for the analyses of coked E-cat samples when a large number of catalyst particles is studied.

Simultaneous in situ Raman and fluorescence (lifetime) microscopy, used to track single E-cat particles during hexane cracking, further clarified the trends observed. The Raman spectroscopy data indicated the growth of polyaromatic species into graphitic carbon, illustrated by an increase in the RTR values. The rate of the graphitization varied considerably from catalyst-particle to catalyst-particle, indicating the broad activity distribution of catalyst particles in an E-cat mixture. The rise and decline of $\overline{\tau}$ confirms the results of the ex situ sample averaged analyses. Moreover, the changing fluorescence dynamics, together with the fluorescence redshift suggested the prolonged presence of smaller coke species of which the fluorescence is quenched more and more by adjacent larger polyaromatics that can act as Förster resonance energy transfer acceptors. The technique developed here was also used to track single coked E-cat particles during their regeneration and revealed the breaking of larger graphitic coke structures, the formation of polyaromatics, and the cleansing of the catalytic surface. These results illustrate that the combined microscopy technique developed in this work can yield new insights in the physicochemical processes occurring within catalyst particles during their coking and regeneration process.

Acknowledgements

B.M.W. acknowledges financial support for this project from the TKI (Top Consortia for Knowledge and Innovation) for Chemistry and BASF, as well as the Dutch Research Council (NWO) in the frame of the Gravitation program Netherlands Center for Multiscale Catalytic Energy Conversion (MCEC). Dr. Stefan Kotrel (BASF) is acknowledged for his useful advice and stimulating discussions. Dennis Hamstra (Albemarle Catalysts, Ketjen) is thanked

for providing the coked E-cat material. Matteo Monai (Utrecht University, UU) is thanked for his role in the supervision of R.F. Sebastian Rejman (UU) is thanked for the TGA measurements.

Conflict of Interest

The authors declare no conflict of interest.

Data Availability Statement

The data that support the findings of this study are available from the corresponding author upon reasonable request.

Keywords: fluid catalytic cracking · in situ spectroscopy · coke formation · fluorescence lifetime microscopy

[1] H. S. Cerqueira, G. Caeiro, L. Costa, F. Ramôa Ribeiro, *J. Mol. Catal. A* **2008**, *292*, 1–13.
[2] E. T. C. Vogt, D. Fu, B. M. Weckhuysen, *Angew. Chem. Int. Ed.* **2023**, *62*, e202300319.
[3] E. T. C. Vogt, B. M. Weckhuysen, *Chem. Soc. Rev.* **2015**, *44*, 7342–7370.
[4] S. C. Cardona, A. Corma, *Appl. Catal. B* **2000**, *25*, 151–162.
[5] Y.-H. Lin, M.-H. Yang, *Thermochim. Acta* **2008**, *470*, 52–59.
[6] I. Vollmer, M. J. F. Jenks, R. Mayorga González, F. Meirer, B. M. Weckhuysen, *Angew. Chem. Int. Ed.* **2021**, *60*, 16101–16108.
[7] M. Veselý, R. Valadian, L. Merten Lohse, M. Toepperwien, K. Spiers, J. Garrevoet, E. T. C. Vogt, T. Salditt, B. M. Weckhuysen, F. Meirer, *ChemCatChem* **2021**, *13*, 2494–2507.
[8] M. Guisnet, P. Magnoux, *Appl. Catal.* **1989**, *54*, 1–27.
[9] D. Mance, J. Van der Zwan, M. E. Z. Velthoen, F. Meirer, B. M. Weckhuysen, M. Baldus, E. T. C. Vogt, *Chem. Commun.* **2017**, *53*, 3933–3936.
[10] U. J. Etim, P. Wu, P. Bai, W. Xing, R. Ullah, F. Subhan, Z. Yan, *Energy Fuels* **2016**, *30*, 10371–10382.
[11] Y. S. Zhang, X. Lu, R. E. Owen, G. Manos, R. Xu, F. R. Wang, W. C. Maskell, P. R. Shearing, D. J. L. Brett, *Appl. Catal. B* **2020**, *263*, 118329.
[12] Á. Ibarra, A. Veloso, J. Bilbao, J. M. Arandes, P. Castaño, *Appl. Catal. B* **2016**, *182*, 336–346.
[13] Q. Almas, M. A. Naeem, M. A. S. Baldanza, J. Solomon, J. C. Kenvin, C. R. Müller, V. Teixeira da Silva, C. W. Jones, C. Sievers, *Catal. Sci. Technol.* **2019**, *9*, 6977–6992.
[14] S. R. Bare, F. D. Vila, M. E. Charochak, S. Prabhakar, W. J. Bradley, C. Jaye, D. A. Fischer, S. T. Hayashi, S. A. Bradley, J. J. Rehr, *ACS Catal.* **2017**, *7*, 1452–1461.
[15] J. Ruiz-Martínez, I. L. C. Buurmans, W. V. Knowles, D. Van Der Beek, J. A. Bergwerff, E. T. C. Vogt, B. M. Weckhuysen, *Appl. Catal. A* **2012**, *419–420*, 84–94.
[16] Q. Qian, J. Ruiz-Martínez, M. Mokhtar, A. M. Asiri, S. A. Al-Thabaiti, S. N. Basahel, B. M. Weckhuysen, *Catal. Today* **2014**, *226*, 14–24.
[17] R. Rieger, K. Müllen, *J. Phys. Org. Chem.* **2010**, *23*, 315–325.
[18] S. J. Strickler, R. A. Berg, *J. Chem. Phys.* **1962**, *37*, 814–822.
[19] M. Y. Berezin, S. Achilefu, *Chem. Rev.* **2010**, *110*, 2641–2684.
[20] J. W. Borst, A. J. W. G. Visser, *Meas. Sci. Technol.* **2010**, *21*, 102002.
[21] M. Sauer, J. Hofkens, J. Enderlein, *Handbook of Fluorescence Spectroscopy and Imaging: From Single Molecules to Ensembles*, Wiley-VCH, Weinheim, **2011**.
[22] A. Einstein, *A. Phys. Z.* **1917**, *18*, 63–77.
[23] D. Patra, *Appl. Spectrosc. Rev.* **2003**, *38*, 155–185.
[24] M. U. Kumke, H.-G. Löhmannsröben, T. Roch, *J. Fluoresc.* **1995**, *5*, 139–152.
[25] J. J. E. Maris, L. A. Parker, K. Stanciakova, N. Nikolopoulos, K. M. H. Berendsen, A. van Blaaderen, F. Meirer, F. T. Rabouw, B. M. Weckhuysen, *Chem. Eur. J.* **2024**, *30*, e202302553.
[26] F. J. Knorr, J. M. Harris, *Anal. Chem.* **1981**, *53*, 272–276.
[27] K.-M. Bark, R. K. Forcé, *Talanta* **1991**, *38*, 181–188.
[28] I. Lezcano-González, R. Oord, M. Rovezzi, P. Glatzel, S. W. Botchway, B. M. Weckhuysen, A. M. Beale, *Angew. Chem. Int. Ed.* **2016**, *55*, 5215–5219.
[29] A. Samoylenko, M. Kögler, A. Zhyvolozhnyi, O. Makieieva, G. Bart, S. S. Andoh, M. Roussey, S. J. Vainio, J. Hiltunen, *Sci. Rep.* **2021**, *11*, 19594.
[30] F. Madonini, F. Villa, *Sensors* **2021**, *21*, 4287.
[31] I. Nissinen, J. Nissinen, A. K. Länsman, L. Hallman, A. Kilpelä, J. Kostamovaara, M. Kögler, M. Aikio, J. Tenhunen, *Eur. Solid-State Device Res. Conf.* **2011**, 375–378.
[32] J. Kostamovaara, J. Tenhunen, M. Kögler, I. Nissinen, J. Nissinen, P. Keränen, *Opt. Express* **2013**, *21*, 31632.
[33] R. Vogel, P. T. Prins, F. T. Rabouw, B. M. Weckhuysen, *Catal. Sci. Technol.* **2023**, *13*, 6366–6376.
[34] R. Boerefijn, N. J. Gudde, M. Ghadiri, *Adv. Powder Technol.* **2000**, *11*, 145–174.
[35] A.-E. Nieuwelink, J. C. Vollenbroek, R. M. Tiggelaar, J. G. Bomer, A. van den Berg, M. Odijk, B. M. Weckhuysen, *Nat. Catal.* **2021**, *4*, 1070–1079.

Manuscript received: May 20, 2024
Accepted manuscript online: July 8, 2024
Version of record online: September 2, 2024